POLITECNICO
MILANO 1863

REPORT Finite Element Modelling

PROJECT NR.3

STENT EXPANSION BY MEANS OF AN ANGIOPLASTY BALLOON

Giacomo Avanzi

Hoseinikhah Seyed Mahdi

Matteo Contardi

Giulia Fischetti

Introduction

Angioplasty is a minimally invasive endovascular surgical procedure widely used to treat arterial atherosclerosis. It consists in the expansion of a polymeric ballon placed into the stenosis tract thanks to a catheter guide, in order to compress the sclerotic plaque and restore the physiological blood flow. To prevent re-stenosis and support the damaged vessel walls, the procedure can be performed in combination with stenting, which is the deployment, by plastic deformation, of a metallic reticular tube in the damaged tract by means of the same ballon expansion. Materials, shapes and dimension of the stent can vary based on treatments and localization of the stenosis.

The purpose of our study was to practice the use of ABAQUS CAE finite elements software by examining the expansion and a subsequent deflation of the balloon inside a stent ring for which both geometries and mechanical properties were provided. The parameters of interest are all related to the uncrimping process of the stent strut, such as longitudinal shortening, radial recoil and plastic strain field.

Materials and Methods

Geometry

Geometries of the stent and the balloon were given as displayed below (Fig. 1-2):

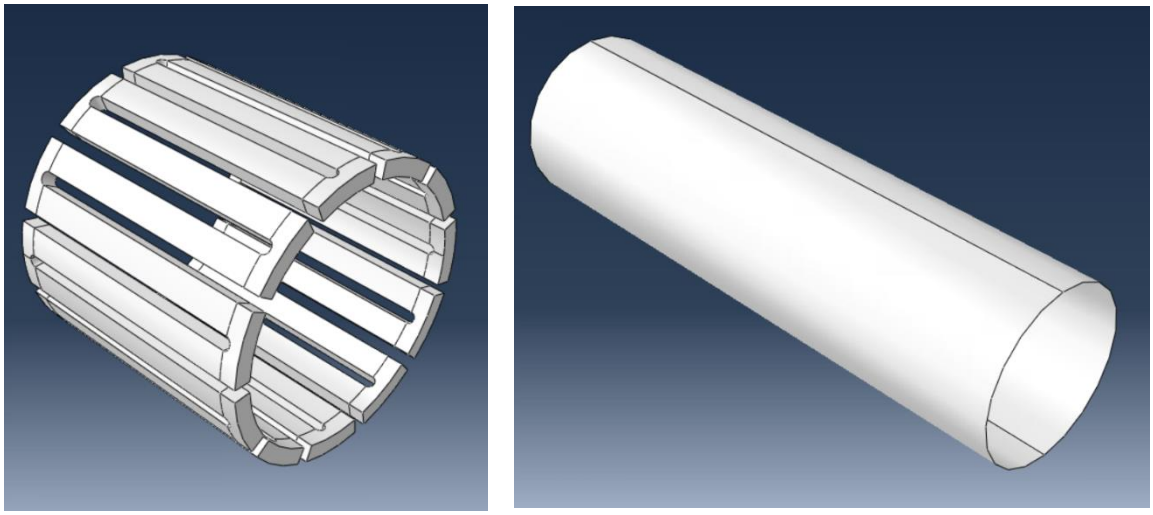

Fig. 1-2: Stent and balloon geometries

As noticeable, the stent ring is composed of 22 repetitive structures, each developing over $\frac{360}{22}$ degrees along θ coordinate, while the balloon features an axisymmetry. As presented in both Liang et al [1] and David et al [2] we can leverage such symmetries to reduce working volumes, contact surfaces and consequently computational cost.

The ring was so cut into a single strut representing one twenty-second of the initial geometry. The balloon was adapted to a slightly wider extent to prevent issues related to the contact model along the cut edge. Contact model on ABAQUS is indeed ruled by normal vectors defined at the nodes, obtained as average of the closest elements' normal. By considering the nodes belonging to one of the edges of the stent in contact with the balloon, their normal vectors are tilted by 45° outwards as average of radial and tangential normals. So, by not considering a slightly larger balloon, those normals might not find a contact element.

Both severings were performed by means of radial planes that were, for the stent, defined using the longitudinal axis and the midpoint of the strut, while for the balloon, defined by the longitudinal axis and an angular extent of 18°, greater than the ≈16,4° extent of the strut section.

Both parts were then placed into an assembly, constraining each other's midplanes and fixing a co-axial constrain, that were later used to define a new cylindrical reference frame (Fig.3).

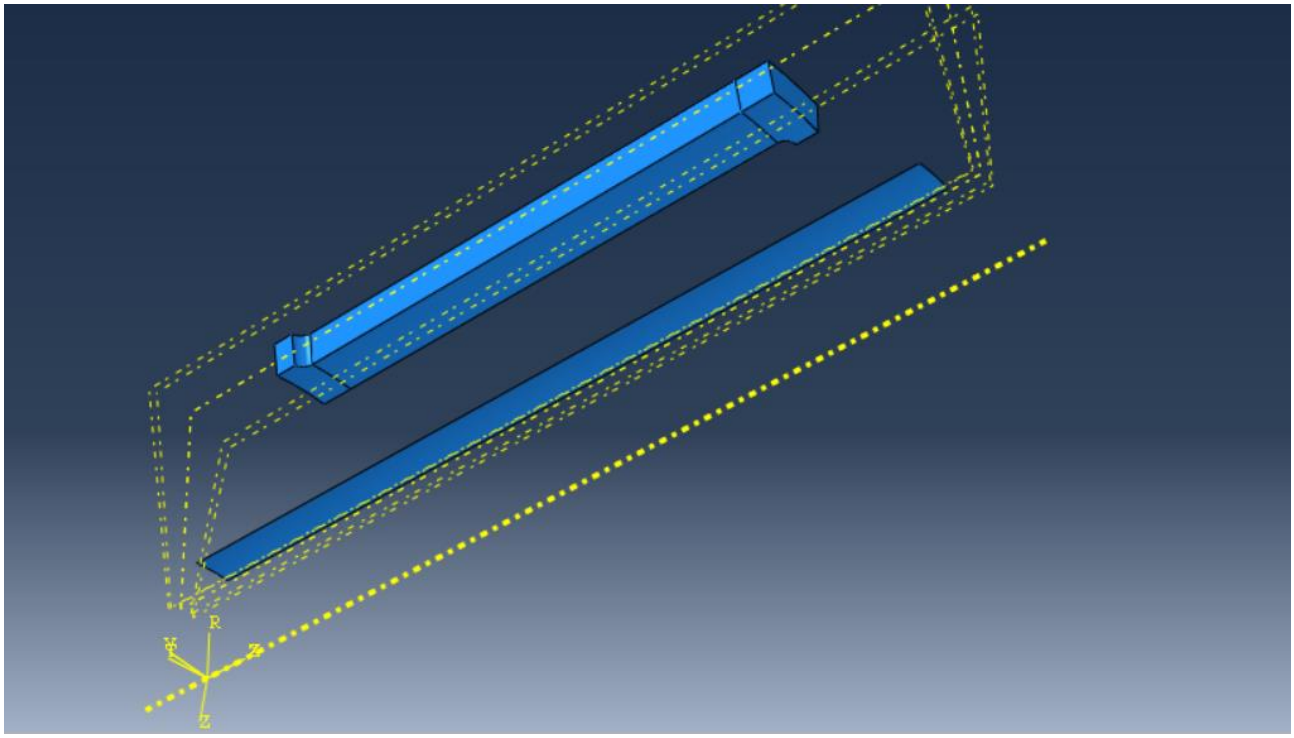

Fig.3: Strut and balloon assembly.

Materials

Material properties for both parts were given as inputs of our project (Tab.1):

STENT - AISI 316 L	
Density	8.0 g/cm^3
Modulus of Elasticity	193 GPa
Yield Tensile Strength (engineering value)	205 MPa
Ultimate Tensile Strength (engineering value)	515 MPa
Elongation at Break (engineering value)	0.6
Poisson ratio	0.3

DELIVERY SYSTEM	
Density	1.256 g/cm^3
Modulus of Elasticity	900 MPa
Poisson ratio	0.3

Tab.1: Material property data.

The ring, with a length of 4,95 mm, an internal radius of 2,276 mm and a thickness of 0,3 mm, is made of AISI 316 L alloy. The stent material is assumed homogeneous, with elasto-plastic characteristics.

When defining plasticity data in ABAQUS, true stress and true strain must be used, seeing that the software requires these values to interpret the data correctly. Since we were given engineering values

for the Yield Tensile Strength, Ultimate Tensile Strength and Elongation at Break, we needed to convert these values into true stress/strain values. For this conversion we used the following relations:

$$\varepsilon_T = \ln(1 + \varepsilon_e) \qquad \sigma_T = \sigma_e(1 + \varepsilon_e)$$

Afterwards, we filled in the Mass Density data by converting the unit measurement from [g/cm^3] to [N s^2/mm^4] and imposing a uniform distribution. This value acquires numerical relevance only in the case where inertial effects are considered (dynamic simulation), in order to assign masses at each element and so, at the nodes. It also affects the convergence of the explicit solver, by modulating the critical Δt by means of the celerity ($C = \sqrt{\frac{E}{\rho}}$). In our case, as explained in next paragraph, we used a static general simulation, so the density has no particular meaning in the solver process.

To characterize the elastic behaviour of the steel, it is only necessary to define the Young's Modulus and the Poisson's Ratio. Meanwhile, for the plastic part, to approximate the stress-strain behaviour of the material, Abaqus needs more data. The first piece of data obtained defines the initial yield stress of the material and, therefore, should have a plastic strain value of zero. The second data obtained defines the ultimate yield stress and the correspondent plastic strain. To get the second value of the plastic strain, we must decompose the total strain value and break into the elastic and plastic strain components. The plastic strain is obtained by subtracting the elastic strain, defined as the value of true stress divided by the Young's modulus, from the value of total strain.

$$\varepsilon_{pl} = \varepsilon_t - \varepsilon_{el} = \varepsilon_t - \frac{\sigma_y}{E}$$

In this way we modelled the stainless steel as bilinear, since, by giving just two points of the curve, ABAQUS interprets it as a line. Over the maximum stress, we chose a constant extrapolation.

The balloon, with an initial radius of 1 mm and a negligible thickness is made of a polymeric material. In the same way we have done for the AISI 316 alloy we filled in the Mass Density Data, imposing a uniform distribution, and to describe the elastic behaviour we filled in the Young's Module and the Poisson's Ratio. Being an elastic material, unlike the other one, there is no need to fill out the plastic section.

Furthermore, we imposed for the AISI 316 L alloy and for the Polymeric material to have an isotropic behaviour.

Boundary Conditions

First of all, we decided to subdivide the simulation in three steps, to have more control over the boundary conditions and contact modelling:

- **Initial**: default step created by Abaqus; we used it to impose kinematic BCs that hold true for both subsequent steps:
  - Since we were using only one part of the whole strut, by exploiting the cylindrical reference frame (r,θ,z), we constrained the nodes belonging to the faces obtained by the severing pre-emptively made, limiting translations along θ axis (those nodes could not exit from (r,z) plane). In this way we allowed both longitudinal shifting, which causes the shortening of the stent, and radial expansion of the geometry. Rotations were not limited since they are already under our control thanks to the other conditions imposed.

  - Moreover, to prevent possible shifting along the z-axis of the whole geometry, by result of forces exchanged during expansion through the contact, we imposed an additional

boundary condition limiting only longitudinal movements of one node of the face closer to the origin. An important remark concerning this constraint is that by oversimplifying the expected deformation of the stent during expansion to prevent the shifting of the whole geometry, one option could be constrain a vertical edge of the strut. This boundary condition though, would significantly modify the strain field as pointed out in the results section (last paragraph).

As a result, we have (Fig. 4):

- $u_\theta = 0$ @ surface A (on both sides)
- $u_z = 0$ @ node B

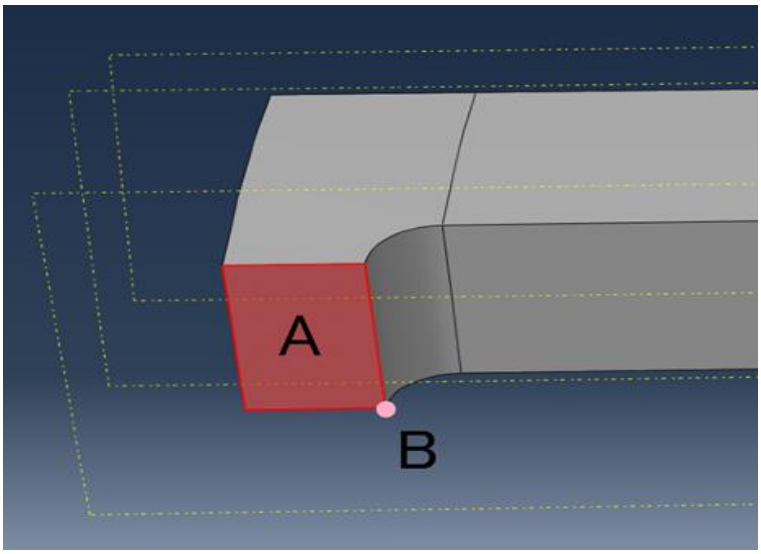

Fig. 4: Explanation of kinematic BCs position.

➢ The balloon was not subjected to any kinematic constraint since it is already being displaced to expand the strut in the next steps.

- **<u>Expansion</u>**: in this step, in order to obtain the plastic deformation of the stent the possible choices were to apply a pressure over the internal surface of the ballon [1][3] or imposing over time, the position of the nodes of the ballon.
  In our study we chose the latter implementation for simplicity but also because we were not considering the actual effects of the expansion on the surrounding artery and plaque; about this topic, for example, Rogers et al [3] conducted an interesting study on the balloon-artery interaction. Moreover, the study was not carried forward to analyze the impact of different BCs [7] on the final shape and apposition of the stent, but it was just a preliminary workbench to learn Abaqus. We are aware that imposing different BCs may yield different results, such as capturing the protrusion of the balloon between the struts, which would instead acquire more relevance when model an actual surgical procedure on an artery-plaque model.
  Loading the balloon with a pressure would also require knowing a certain magnitude to displace the nodes by the correct amount: a trial and error isn't acceptable to find an exact value; Hongxia et al [7] used a binary-search method to do this, since an analytical solution is not possible because of non-linearities and stent-geometry dependence of the radial stiffness.

We exploited again the cylindrical reference frame by imposing over a Δt of 0.1 seconds a linear radial displacement of the entire set of nodes of the balloon, from the initial diameter to the required diameter of 11 mm.

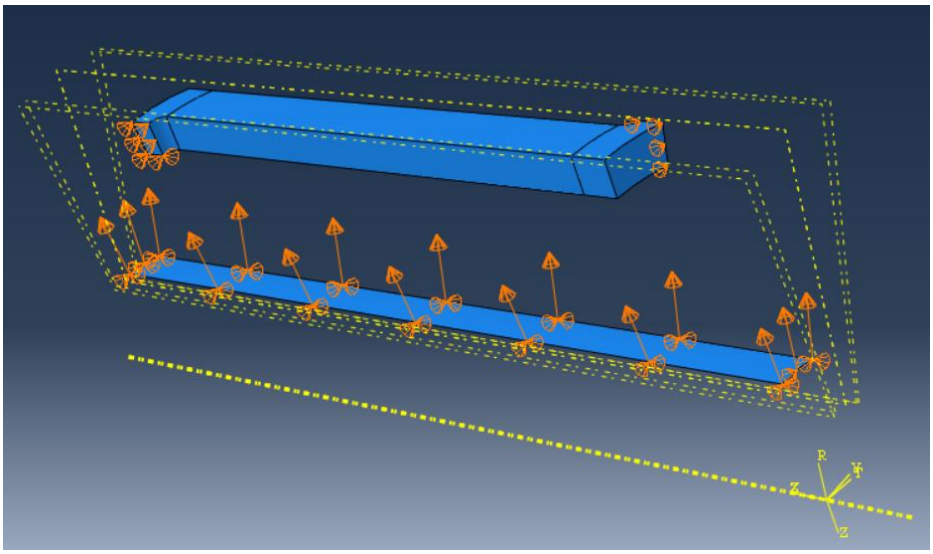

Fig. 5: Visual representation of boundary conditions.

- **Deflation**: over the same period of time of 0.1 s, we imposed once again a linear radial shifting to all the nodes of the balloon up to a final diameter of 6 mm, already over the conclusion of contact between the two parts.

Both expansion and deflation steps were defined as **Static General**, using an implicit (non-linear geometry) simulation, as chosen by Liang et al [1], this choice was motivated by the fact that both parts have a low inertia due to the limited mass and consequently, inertial effects, captured by a dynamic simulation could be, as a first approximation, neglected. This choice has a couple of implications that are highlighted in the following.

Contact Modelling

Due to the intrinsic concept of the angioplasty surgical technique, during expansion and deflation steps it is necessary to implement a contact model between the outer surface of the balloon and the inner one of the struct.

We decided to use a "surface-to-surface" contact, defining main and secondary surfaces as struct and balloon, respectively. We adopted a small sliding formulation, since we were not considering a problem where one node could change dramatically its neighbours on the other surface: the list of possible contacting nodes remained basically the same throughout the process. We also excluded shell element thickness to avoid an excessive unwanted expansion of the stent over the target dimension.

As contact property options, we set:

- a **frictionless** formulation for the **tangential behaviour** as found in literature [1][3], seemed the most suitable choice for our project.
- a default **hard contact** model for the **normal direction**, where separation after contact was obviously allowed to let the balloon detach from the struct during deflation. We opted for hard contact since this choice should be preferred when possible because the pressure-overclosure relationship is the most realistic one: when surfaces are in contact, any contact pressure can be transmitted between them (Lagrangian multiplier). Separated surfaces come into contact

when the clearance between them reduces to zero and separate if the contact pressure reduces to zero [ABAQUS Analysis User's Manual (30.1.2)].
This choice also does not introduce approximations and extra-stiffnesses like the penalty contact. In our case it was a suitable option because it was not a very complex surface contact as the number of contacting nodes was limited, and the choice of static simulation implied not having to consider inertia associated with nodes themselves.

Mesh – Finite Elements

The first step of our workflow was to identify an acceptable meshing technique and an associated dimension of the elements, in order to obtain reliable values for the quantity we needed. Before conducting the actual sensitivity analysis, we conducted some preliminary simulations, to identify a general pattern of stresses and strains and the most critical parts on the stent structure. We assigned linear hexahedral elements C3D8 for the struct and quadrangular shell elements S4R for the balloon.

We assigned the elements of the **balloon** to the shell family (structural elements): these are used to model structures in which one dimension (the thickness) is significantly smaller than the other dimensions and the stresses in the thickness direction are negligible and are not evaluated by the solver.

The **strut** belongs to the Continuum elements family because its topology (3D) and the dimensionality of the problem (3D) coincide: all the possible strain fields are derived only from translational degrees of freedom of the nodes, unlike the shell case, where rotational DOFs must be accounted for.

As noticeable in the following figures (Fig. 6-7), stresses and strains are concentrated around the extremities of the strut, as expected: when the stent is uncrimped, it basically enlarges radially, incrementing the angle between the adjacent struts belonging to the same ring. This stress pattern is a result of this bending moment which is maximum at the connection between the struts.

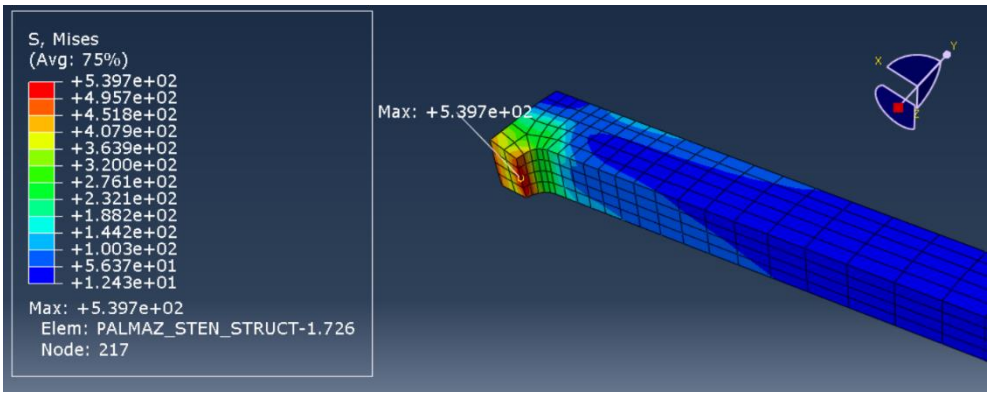

Fig. 6: Von Mises Stress (linear elements).

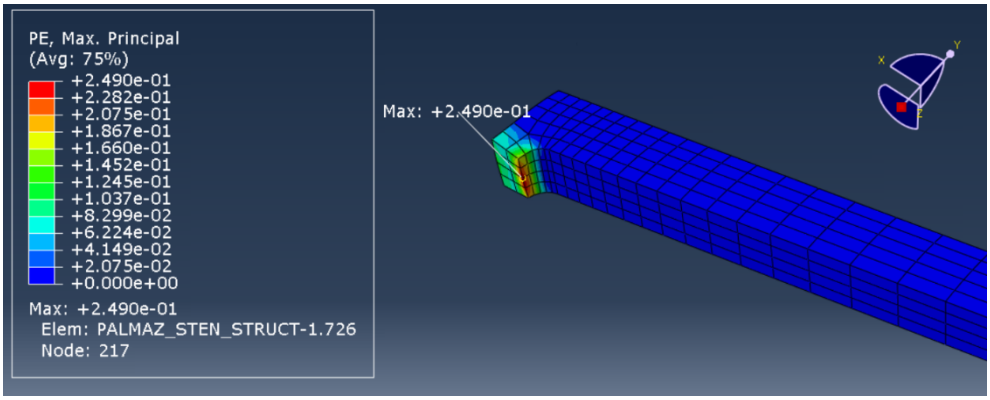

Fig. 7: Plastic Strain Field (linear elements).

Afterwards, we chose some finer element type for the strut discretization: C3D20. The use of a 20-node quadratic element (3 nodes for each side of the hexahedra) with full integration, ensures high accuracy in capturing stress concentrations and detailed deformation behavior. We did not change the element type for the balloon: we are not interested in its strain-stress behavior and removing reduced integration would only, although slightly, increase the computational cost.

Meshing rule

By considering a rather negligible gradient of stresses in the central tract of the strut, and so by focusing on plastic deformation and stresses only in the distal tracts, we decided to partition the strut in three regions: two mirrored distal ends and a central part, and then to proceed as following:

- **Distal region**: given the simplicity of the whole simulation and expecting a rather quick convergence of results, we opted to implement a meshing rule which would increase radial and circumferential number of elements linearly. Considering the surface between central and distal regions, we initially seeded the edges maintaining the dimensional ratio between the two (obtainable using in circumferential direction one element more than radially). We then applied the resulting average dimension to seed the whole distal region with the approximate element size tool, to maintain sort of cubic elements. We set the curvature control “maximum deviation factor” to 0.04 to make sure to correctly capture the fillet.
- **Central tract**: for the whole sensitivity analysis we maintained a rather coarse mesh longitudinally while adapting radially and circumferentially to the distal dimension of elements, that were the ones of our interest. We performed that by seeding the four longitudinal edges with a double bias (minimum size 0.07 mm, maximum size 0.3 mm).

For the ballon instead, by using an implicit static simulation we were not forced to have a correct correspondence between the sizes of the elements of the two contact surfaces: this is something to be aware of only in dynamic cases, where inertial effects would create problems due to the different masses of the nodes. Despite this fact, we could not use a very coarse mesh on the θ-direction or throughout the expansion its surface would be too distorted and wouldn’t resemble a circumference arc, but a polyline. Our rule was to seed longitudinally with a bias, similar to the strut one.

Discussion of results

Mesh sensitivity analysis

We performed several simulations, making use of the meshing rule explained. We started by setting 2 elements along the radial development of the strut (thickness, identified by letter “R”) and 3 elements along circumferential direction (strut width, letter “T”).

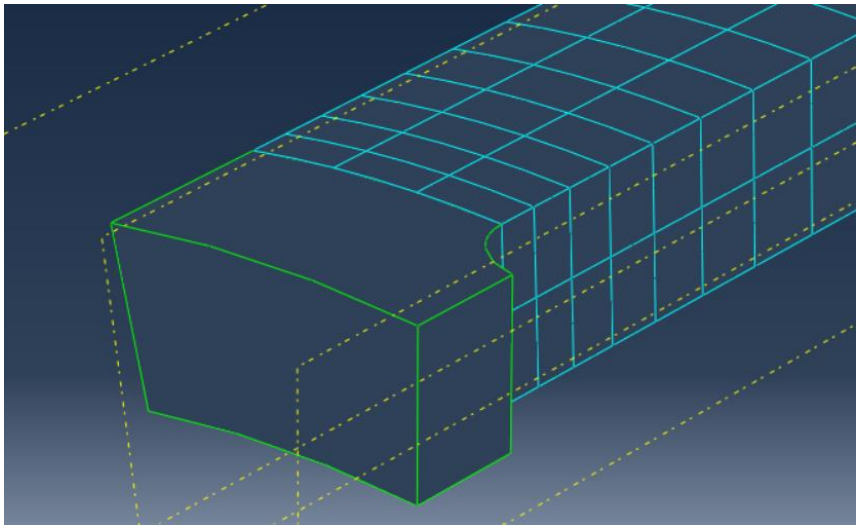

Fig.8: R2-T3 mesh for central part.

We linearly increased one by one R and T number of elements (up to 13 and 14 respectively), always maintaining one element more in θ direction because it helped keeping a squared non-distorted element shape and extracted all quantities of interest for our sensitivity analysis (Tab.2).

We observed that “global” outputs as recoil and shortening converge very quickly (even a very coarse mesh yields more than acceptable results), on the other hand, “local” quantities like Von Mises Stress (VMS) and plastic strains need finer meshes to converge. Despite this fact, coarse meshes (apart from the first one) yield quite acceptable results even for VMS and plastic strains: we must remember that we chose a C3D20 full-integration brick, so for each element side we have 3 nodes and an accurate integration.

To further highlight the difference between convergences among what we called “global” and “local” quantities, we repeated simulations with C3D8 elements, noticing an almost immediate convergence for shortening and recoil data as opposed to Maximum Von Mises Stresses and Plastic Deformations (Tab.3).

To better visualize results we generated the convergence plots of the four parameters, with respect to the elements size (Graphs 1-4).

Job Name	Maximum Plastic Strain [-]	Recoil %	Shortening %	Max VMS [MPa]	Approximate Element Size [mm]
R2-T3	0,3514	2,24	3,77	680,3	0,170
R3-T4	0,3153	2,25	3,74	632,5	0,127
R4-T5	0,3204	2,19	3,76	638,8	0,102
R5-T6	0,3191	2,19	3,78	634,4	0,085
R6-T7	0,2987	2,14	3,80	606,9	0,073
R7-T8	0,3049	2,12	3,82	616,2	0,064
R8-T9	0,3037	2,13	3,81	615,3	0,057
R9-T10	0,2949	2,14	3,83	597,3	0,051
R10-T11	0,3050	2,12	3,81	621,3	0,046
R11-T12	0,3083	2,12	3,81	624,7	0,042
R12-T13	0,3054	2,12	3,81	618,7	0,039
R13-T14	0,3103	2,10	3,84	628,1	0,036

Tab.2: Recap of mesh sensitivity analysis results using C3D20 elements.

Job Name	Maximum Plastic Strain [-]	Recoil %	Shortening %	Max VMS [MPa]	Approximate Element Size [mm]
R2-T3	0.2025	1.96	3.81	515.1	0.170
R3-T4	0.2655	2.01	3.31	565.3	0.127
R4-T5	0.249	2.01	3.82	539.7	0.102
R5-T6	0.252	2.06	3.82	542.3	0.085
R6-T7	0.2571	2.01	3.86	548.7	0.073
R7-T8	0.2699	1.93	3.81	534.7	0.064
R8-T9	0.2793	2.03	3.83	579.9	0.057
R9-T10	0.2752	1.98	3.80	574.9	0.051
R10-T11	0.2862	1.96	3.82	587.3	0.046
R11-T12	0.2895	2.04	3.82	595.8	0.042
R12-T13	0.2869	2.03	3.82	591.1	0.039
R13-T14	0.2861	2.14	3.80	591.5	0.036
R14-T15	0.2904	2.13	3.82	596	0.034

Tab.3: Recap of mesh sensitivity analysis results using C3D8 elements.

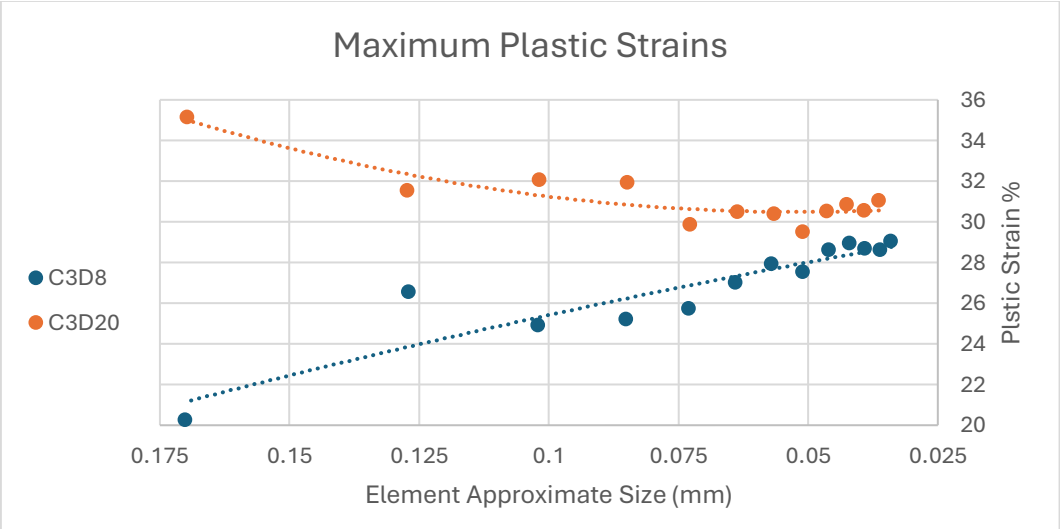

Graph 1

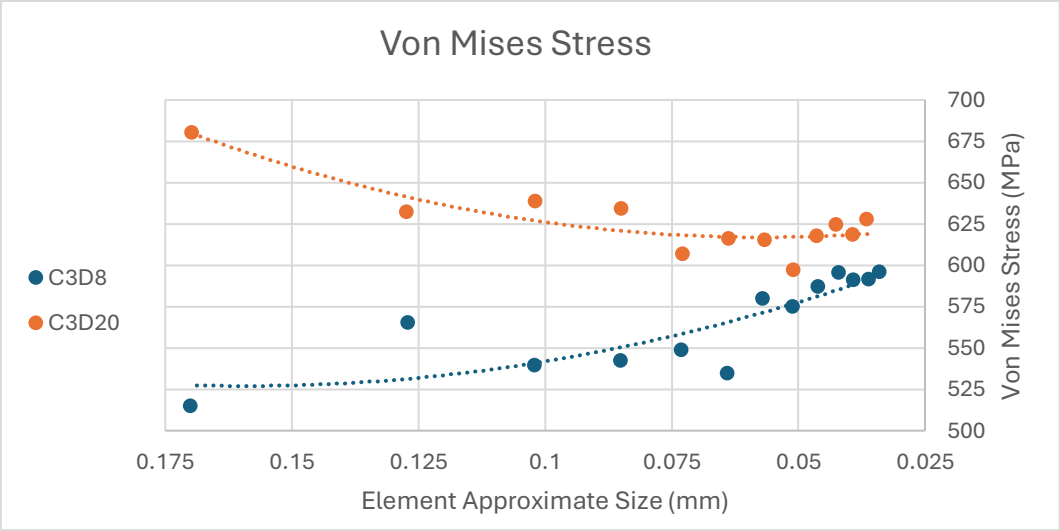

Graph 2

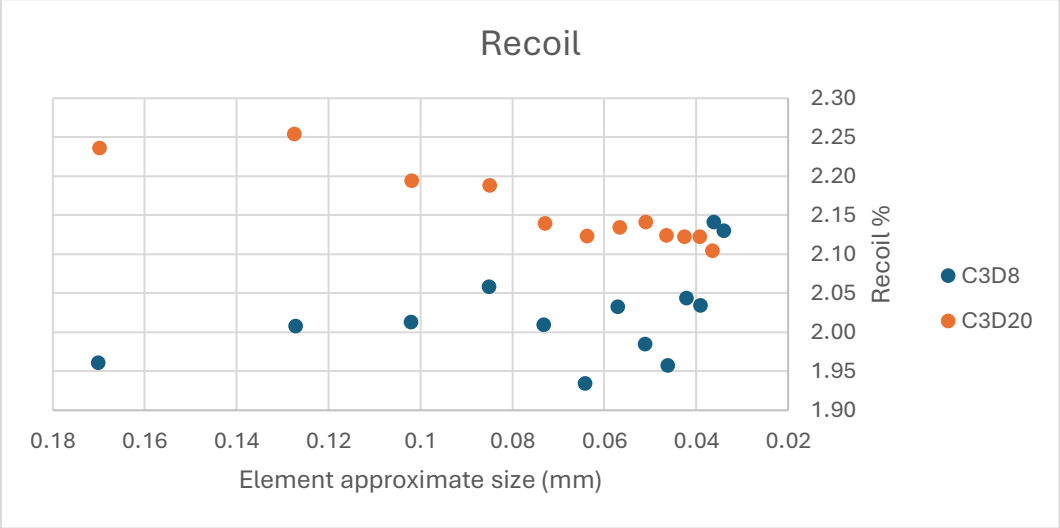

Graph 3

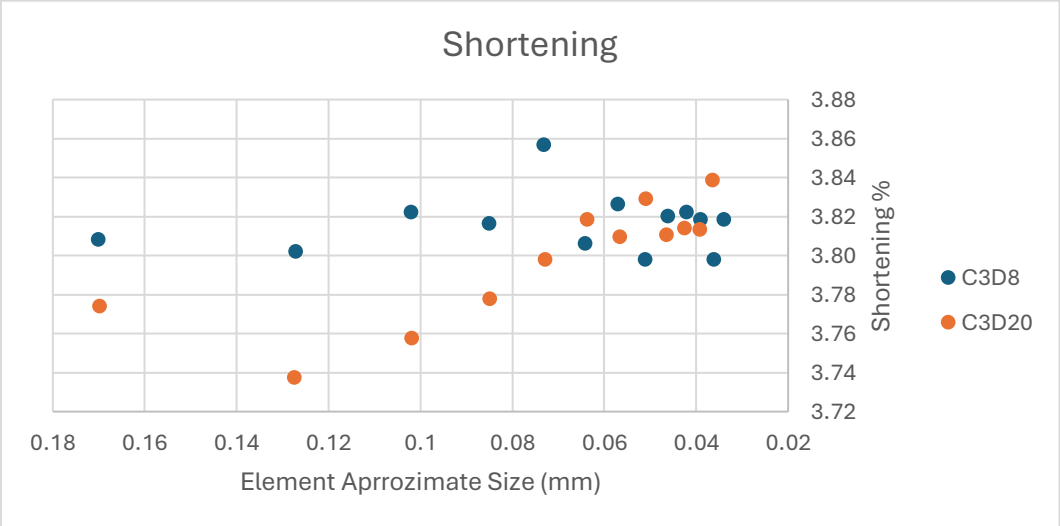

Graph 4

Plastic strain and VMS fields

Considering the sensitivity analysis conducted, we concluded that "R10-T11" simulation ($approximate\ element\ size\ =\ 0.046\ mm$) seems the best compromise between accuracy and computational cost. Increasing even more the number of elements, we do not detect significant differences in the results. Regarding the local quantities of our interest, we get:

- Maximum Plastic Strain = 30.5 %
- Maximum Von Mises Stress = 621,3 MPa

The associated fields can be seen in figures 9-10.

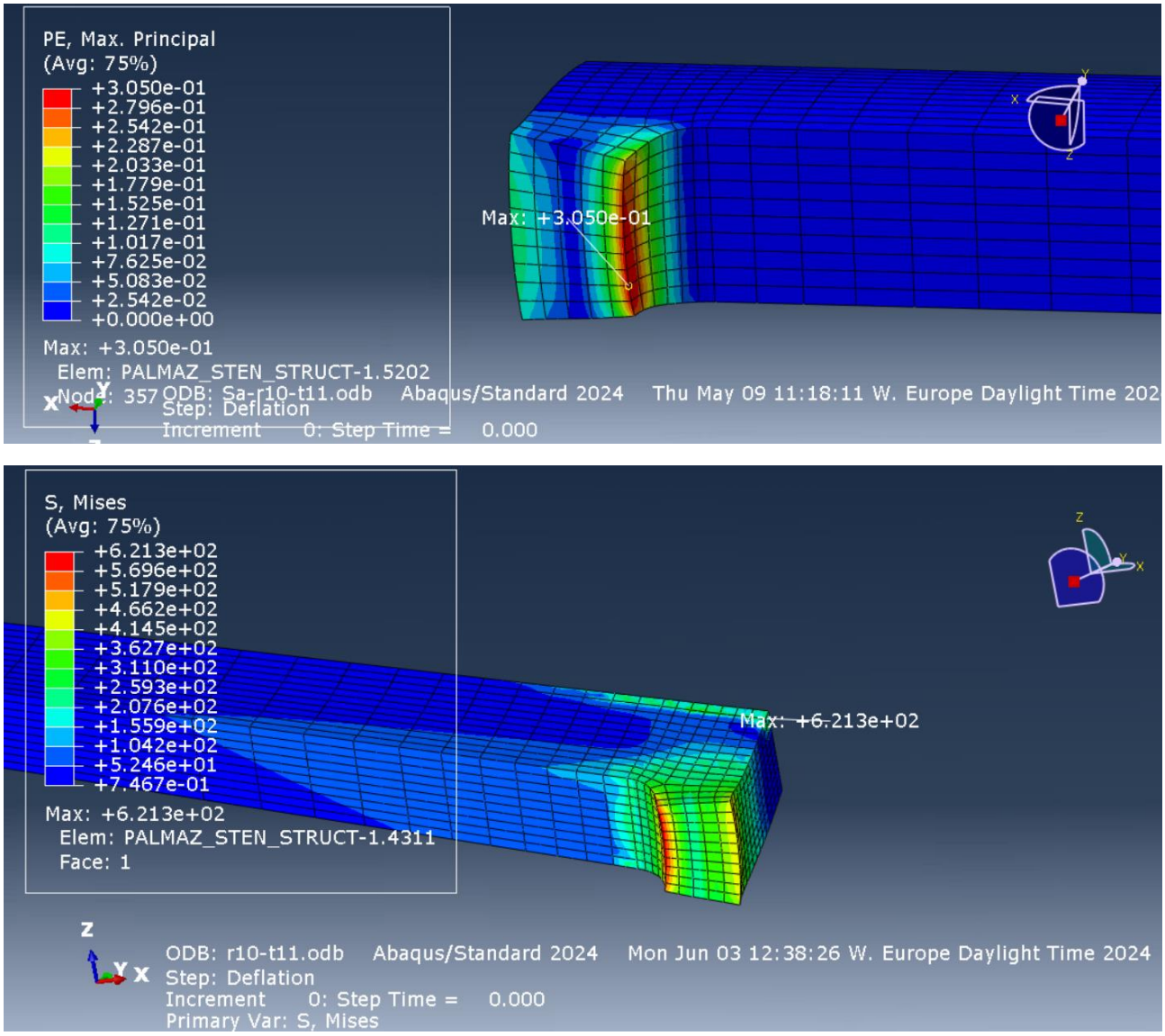

Fig.9-10: Plastic strain and VMS fields with a fine mesh.

Looking at the distribution of plastic strains (for VMS it would be similar) over the two critical edges we get (Fig.11):

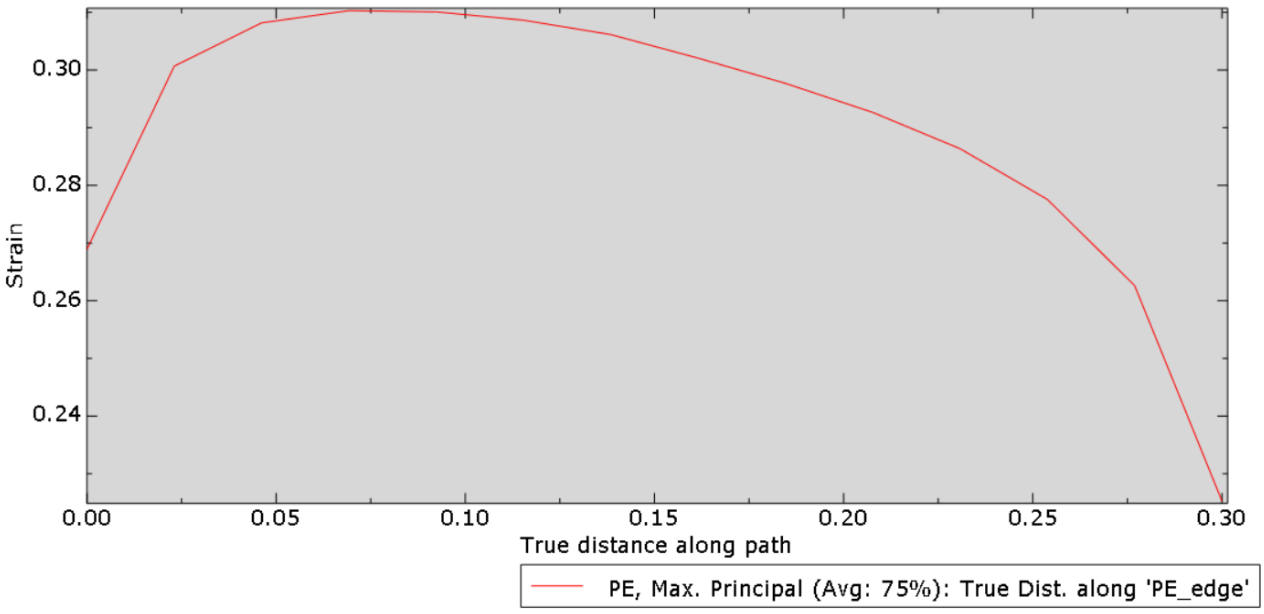

Fig.11: Plastic strain over critical edges.

Recoil and shortening

When the balloon deflates and returns to its initial state, the diameter of the stent also decreases accordingly, so it's relevant to our project to analyze the recoil ratio of the strut. The Recoil ratio can be calculated as the percentage difference between the mean internal diameter of the strut at the end of the expansion and at the end of the deflation:

$$Recoil\ Ratio = \frac{D_{\mathrm{inf}\,lated} - D_{deflated}}{D_{\mathrm{inf}\,lated}} \times 100$$

To be more accurate to get $D_{\mathrm{inf}\,lated}$ we extrapolated three values of diameters at the end of expansion, on the inner side of the strut (for different θ positions) and obtained an average of them. The same rationale was used to evaluate D_{deflated}.

In our study, the recoil ratio is approximately 2.12%. It is important to note that this value is significantly lower than what is observed in practical applications. If a real artery and a potential plaque were included in the model, the radial stress on the stent after balloon deflation would be considerably higher. To emphasize this effect, we can compare our results to the literature, as shown in the following table (Tab.4), the recoil ratio obtained by Liang et al. [1] is reasonably close to our findings. However, when considering the influence of the artery and plaque, this ratio would be approximately three times greater.

Model	Recoil Ratio(%)	Reference
Balloon-Stent	2.1	Our Study
Balloon-stent	3.1	Liang et al [1]
Balloon-stent-plaque-artery	6.4	Chen et al [5]

Tab. 4: Recoil Ratio (%)

We calculated the shortening as the percentage difference between the longitudinal length at the initial state and the deformed longitudinal length at the end of the deflation. As a general rule, we got these values querying the z-distance between two points at half thickness belonging to the cut faces.

$$Shortening = \frac{(L_{initial} - L_{final})}{L_{initial}} \times 100$$

In our study, the shortening converges quickly to the approximate value of 3,81%.

Implications of numerical deployment time

In our simulation, the expansion step lasts 0.1 seconds. This Δt can be changed, as in real applications this deployment time could be different. From a numerical standpoint, this quantity changes only the velocity through which the balloon nodes are displaced; we are indeed applying a linear displacement along radial coordinate from 1 [mm] to 5.5 [mm]: if this process is concretized in a longer time span, a smaller slope in the displacement-time plot is obtained.

This change could only have some effects, in terms of results yielded, in a dynamic simulation where, the use of a very small deployment time would lead to an over-expansion of our parts due to the inertia gained in the displacement, although, as already said we are not capturing this behaviour (Fig.12).

The only thing noticeable when incrementing deployment time, leaving unchanged the maximum dt allowed and the maximum number of increments in the steps solving, is a possible abortion of the simulation due to exceeding the latter.

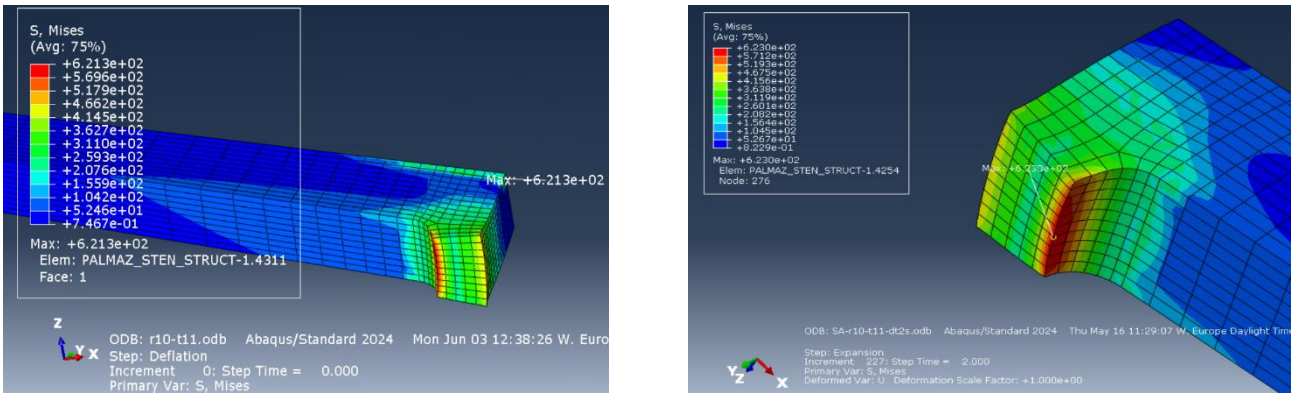

Fig.12: No difference in using Δt equal to 0.1 s (left) and 2 s (right) in a static general simulation.

Comment on kinematic BC on the stent

As explained in Materials and Methods, if we had placed an axial constraint on the whole vertical edge of the strut, we would have compromised the natural strain fields on the distal tracts.

This is one effect that we wouldn't have expected from the beginning: the stresses resulting from the contact with the balloon, in the distal part cannot be considered as only a momentum that tends to open up the crimped struct (a bending in the plane tangent to the circumference), but a more complex stress field including a deformation in the r-z plane (Fig.13). This behaviour does not come from the choice of a radial displacement of the balloon as a computational trick to expand it: from an auxiliary simulation conducted imposing a pressure directly on the in inner strut surface (to exclude contacts), we get the same curvature effect (Fig.14).

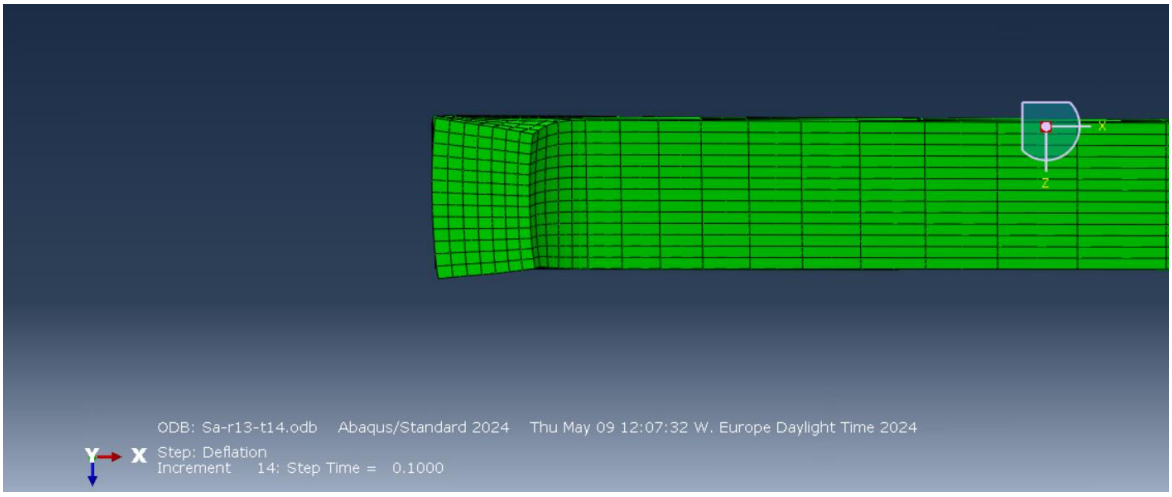

Fig.13: Curvature on the r-z plane of the junction between two struts of a ring.

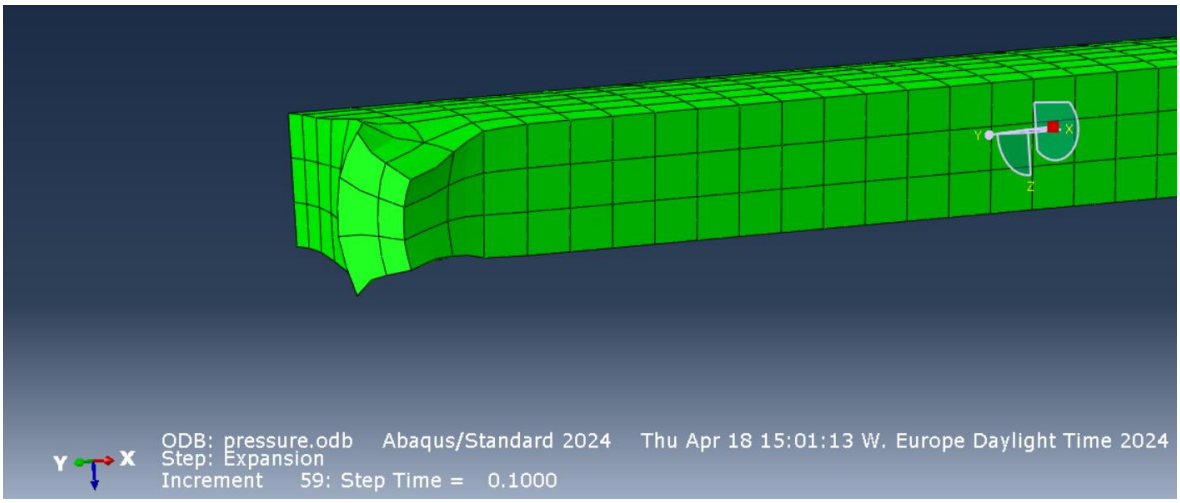

Fig.14: Same curvature but obtained with a pressure. The effect is exaggerated to make it clearer (in this example radial coordinate of inner nodes is 15.6 mm instead of 5.5 mm).

Bibliography

[1] D.K. Liang, D.Z. Yang, M. Qi, W.Q. Wang. Finite element analysis of the implantation of a balloon-expandable stent in a stenosed artery (doi:10.1016/j.ijcard.2004.12.033)

[2] David Chua SN, Mac Donald BJ, Hashmi MSJ. Finite element simulation of stent and balloon interaction. J Mater Process Technol 2003;143-144:591 – 7

[3] Campbell Rogers, David Y. Tseng, James C. Squire, Elazer R. Edelman. Balloon-Artery Interactions During Stent Placement A Finite Element Analysis Approach to Pressure, Compliance, and Stent Design as Contributors to Vascular Injury (Circ Res. 1999;84:378-383.)

[4] ABAQUS Analysis User's Manual: https://classes.engineering.wustl.edu/2009/spring/mase5513/abaqus/docs/v6.6/books/usb/book01.html

[5] SL Chen, NS Guo, HD Chen - Radiology Research and Practice, 2001. The immediate elastic recoil of percutaneous coronary angiography and intracoronary stent implantation.

[6] Getting Started with Abaqus - Interactive Edition - Version 6.8

[7] Hongxia Li, Tianshuang Qiu, Bao Zhu, Jinying Wu, and Xicheng Wang. Design Optimization of Coronary Stent Based on Finite Element Models (https://doi.org/10.1155/2013/630243).